1 Equations

Kernel correlation

To calculate the Kernel correlation we use Fourier transforms for profiles

$$f(x) = \sum_k f_k^* \psi_k^*(x); \quad g(x) = \sum_l g_l \psi_l(y); \quad \rho = \sum_m \rho_m \psi_m(x-y) \tag{1}$$

where $\psi_k(x) = e^{2\pi ikx/L}$; $\psi_k^*(x) = e^{-2\pi ikx/L}$; * means Complex conjugate; L – genome length.

$$Q_\rho(f,g) = \int\limits_G \int\limits_G f(x)g(y)\rho(x-y)dxdy = \int\limits_G \int\limits_G \sum_k f_k^* \psi_k^*(x) \sum_l g_l \psi_l(y) \sum_m \rho_m \psi_m(x-y)dxdy \tag{2}$$

Note, that

$$\psi_m(x-y) = \psi_m(x) \cdot \psi_m^*(y) \tag{3}$$

Then the Eq.(2) can be rewritten as:

$$\begin{aligned} Q_\rho(f,g) &= \textstyle\sum_{k,l,m} f_k^* g_l \rho_m \int\limits_G \int\limits_G \psi_k^*(x)\psi_l(y)\psi_m(x)\psi_m^*(y)dxdy \\ &= \textstyle\sum_{k,l,m} f_k^* g_l \rho_m \int\limits_G \psi_k^*(x)\psi_m(x)dx \int\limits_G \psi_l^*(y)\psi_m^*(y)dy \end{aligned} \tag{4}$$

The basis functions ψ_k are orthogonal:

$$\int\limits_G \psi_k(x)\psi_m^*(x)dx = \begin{pmatrix} 1, & k = m \\ 0, & k \neq m \end{pmatrix} = \delta_{k,m} \tag{5}$$

Finally we have:

$$Q_\rho(f,g) = \sum_{k,l,m} f_k^* g_l \rho_m \delta_{k,m} \delta_{l,m} = \sum_k f_k^* g_k \rho_k \tag{6}$$

Cross-correlation

The cross-correlation function is:

$$c(x) = \frac{1}{\sigma_f \sigma_g} \frac{1}{|G|} \int\limits_G f(t)g(t-x)dt \tag{7}$$

Using Fourier transformation we can write

$$\int\limits_G f(t)g(t-x)dt = \int\limits_G \sum_k f_k \psi_k(t) \sum_m g_m^* \psi_m^*(t-x)dt \tag{8}$$

Using decomposition (3) and orthogonality (5) we obtain:

$$\begin{aligned} \int\limits_G f(t)g(t-x)dt &= \int\limits_G \textstyle\sum_k f_k \psi_k(t) \sum_m g_m^* \psi_m^*(t)\psi_m(x)dt \\ &= \textstyle\sum_k \sum_m f_k g_m^* \psi_m(x) \int\limits_G \psi_k(t)\psi_m^*(t)dt = \sum_k f_k g_k^* \psi_m^*(x) = FT^{-1}(f_k g_k^*) \end{aligned} \tag{9}$$

where FT^{-1} means reverse Fourier transform. Finally we obtain equation for the cross-correlation function;

$$c(x) = \frac{1}{\sigma_f \sigma_g} \frac{1}{|G|} FT^{-1}(f_k g_k^*) \tag{10}$$

Local Correlation

The local correlation is based on calculation of the integral $\int\limits_G \rho(x-t)f(t)dt$. Doing the Fourier transform for $f(t)$ and $\rho(x-t)$ we obtain:

$$\int\limits_G \sum_{k,m} \rho_m \psi_m(x-t) f_k \psi_k(t) dt = \sum_{k,m} \rho_m f_k \psi_k(x) \int_G \psi_m^*(t)\psi_k(t)dt = FT^{-1}(\rho_k f_k) \tag{11}$$

2 Example of output plots

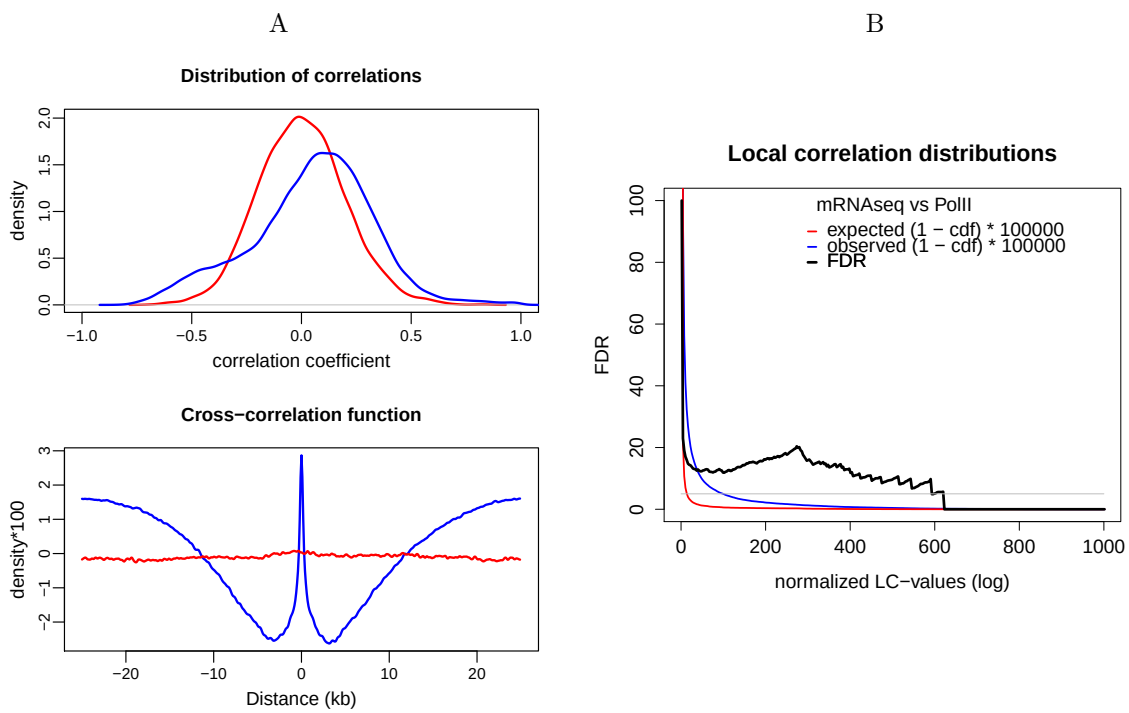

Figure S1: A. Example of output plots: H3K27me3 vs H3K36me3 in Fetal brain cells. The upper plot shows the distribution of the Kernel Correlations over the windows; the lower plot shows the cross-correlation function. Red lines reflects the background distribution; blue line – the matched windows B. Distributions of the local correlations for mRNA Seq vs PolII in IMR90 cell line. Red line – background distribution $(1-cdf)$; Blue line – observed distribution $(1-cdf)$; Black line – FDR.

3 Partial Correlations

We take two epigenomic tracks (repressive polycomb-related H3K27me3 and active promoter-related H3K4me3) and the input track and the nucleosomes track as confounders for GM12878 cell line. The results are presented on the Fig. S2. These tracks are positively correlated with input and nucleosome tracks (Fig. S2A-D). We observe a significant positive correlation of these tracks if we do not use projection mode(Fig. S2E). Usage the input track or nucleosome track as confounders remove the positive correlation (Fig. S2F-G). But if we use the nucleosome track as a confounder the correlation distribution became very close to the background distribution with a tail at the positive values. Moreover, there exists a not high narrow peak at zero correlation. In this case, this peak may reflect 'poised promoters' or difference of the epigenomic status in homologous chromosomes.

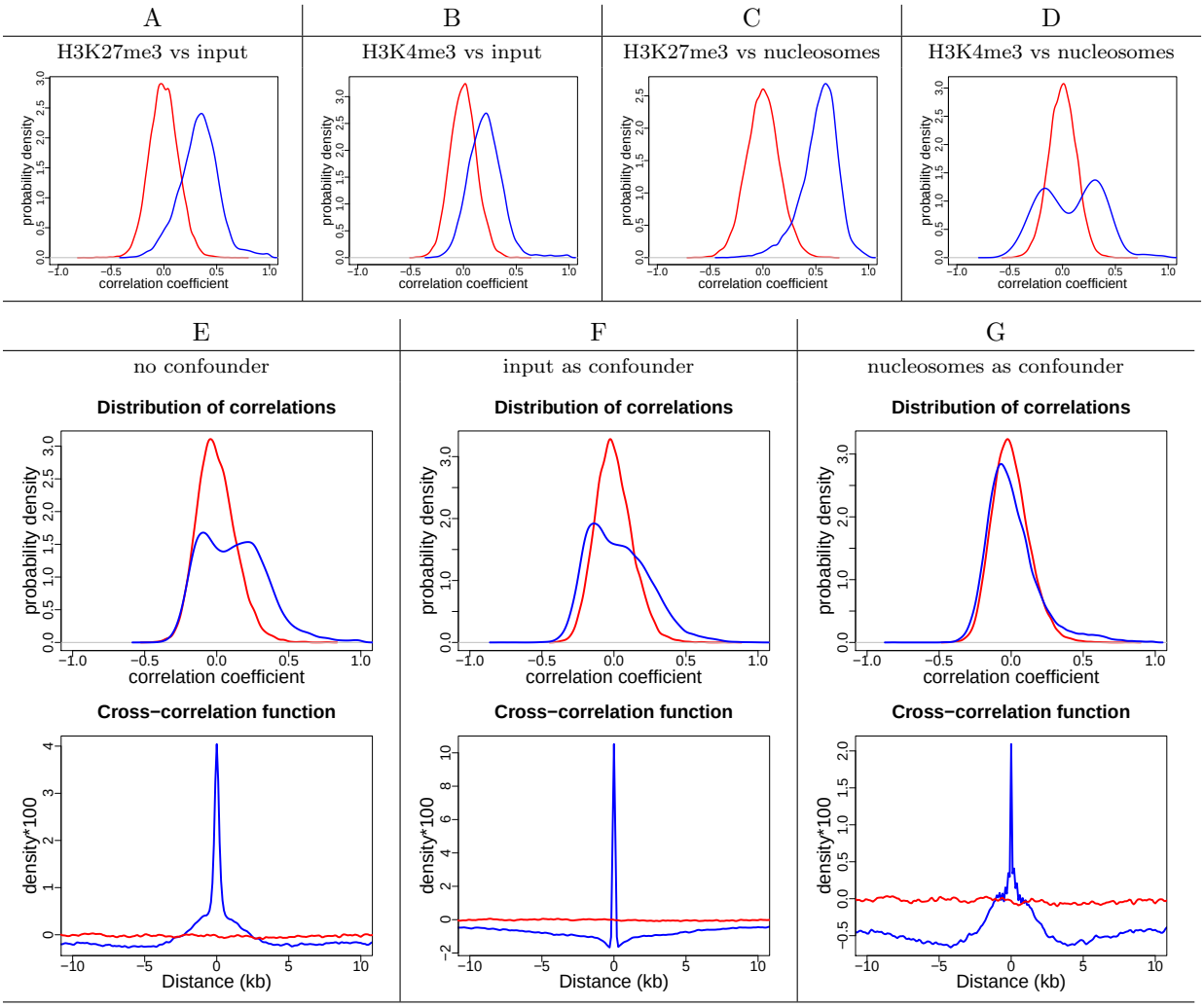

Figure S2: The correlation distributions for H3K36me3 track vs H3K4me3 track in GM12878 cells. Figures E-G also contain a cross-correlation functions (bottom plot). A. – H3K27me3 vs input; B. – H3K4me3 vs input; C. – H3K27me3 vs nucleosomes; D. – H3K4me3 vs nucleosomes; E. – H3K27me3 vs H3K4me3 without confounder; F. – H3K27me3 vs H3K4me3 with the input track as confounder; G. – H3K27me3 vs H3K4me3 with the nucleosome track as confounder

4 The cross-correlation functions for comparison of epigenomic tracks vs gene features

We select main epigenomic methylation tracks for Brain Cingulate Gyrus. Then we take RNA-seq data for this cell type and divide all genes by expression level by three categories: high expressed genes (top 25%) low expressed genes (bottom 25%) and medium expressed genes. For these genes using refseq we prepare three tracks with the gene annotations. Next we run *StereoGene* to compare every epigenomic track with every gene track using the interval flags `-gene_beg, -gene_end, -ivs_beg, -ivs_end`. The resulting cross-correlation functions are presented on the Fig.S3.

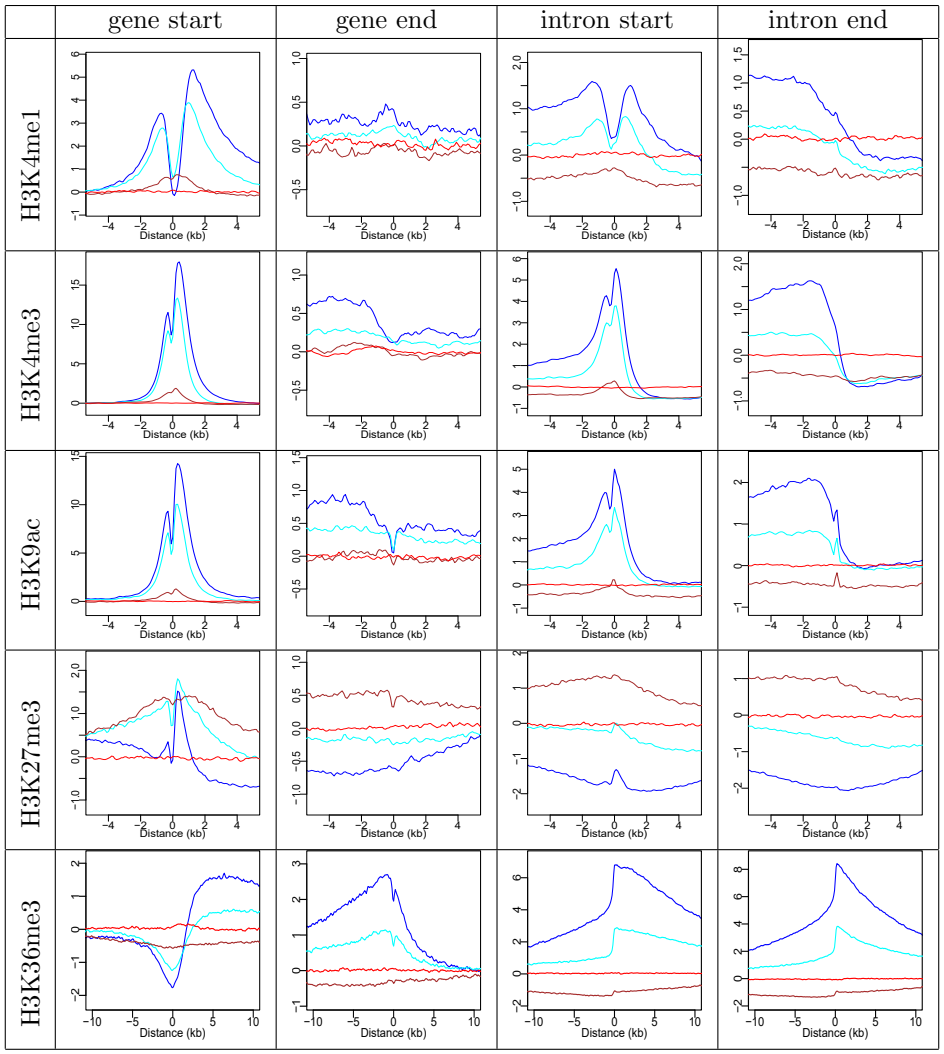

Figure S3: Cross-correlation functions for different epigenomic marks and gene features. Blue line – active genes (top 25%); Cyan line – middle expressed genes Brown line – silent (bottom 25%) genes Red line – background cross-correlation function

5 Interaction of the cohesine Rad21 with chromatin marks and CTCF

We apply the *StereoGene* to compare binding of the cohesine protein Rad21 with chromatin marks and CTCF binding sites. the results presented on the Table S1

Table S1: Correlations of cohesin Rad21 track vs histone modifications

Cohesin	Feature	avCorr	p-value
H1 stem cells			
Rad21	H3k9me3	0.013	3.0E-019
Rad21	H3k36me3	0.026	2.5E-038
Rad21	H3k79me2	0.040	4.2E-146
Rad21	H2az	0.104	0
Rad21	H4k20me1	0.104	0
Rad21	H3k27me3	0.105	0
Rad21	H3k27ac	0.127	0
Rad21	H3k9ac	0.150	0
Rad21	H3k4me3	0.169	0
Rad21	H3k4me1	0.197	0
Rad21	H3k4me2	0.212	0
Rad21	CTCF	0.914	0
K562 cell line			
Rad21	H3k36me3	0.004	0.05
Rad21	H3k27me3	0.021	6.0E-032
Rad21	H3k9me3	0.081	0
Rad21	H3k9me1	0.111	0
Rad21	H4k20me1	0.128	0
Rad21	H3k4me1	0.139	0
Rad21	H3k79me2	0.146	0
Rad21	H3k27ac	0.146	0
Rad21	H3k9ac	0.161	0
Rad21	H2az	0.179	0
Rad21	H3k4me3	0.185	0
Rad21	H3k4me2	0.197	0
Rad21	CTCF	0.615	0

6 CAGE vs gene annotation

We analyzed the positional relationship of CAGE data, a genome-wide map of capped mRNA, for the nucleus and for cytosole of H1-hESC cells and the RefSeq gene annotations. The cross-correlation functions are presented in Fig. S4. CAGE clusters are highly correlated with transcription start sites (Fig. S4A), as expected. In addition, we observed two unexpected phenomena: strong positional correlation of CAGE clusters (panel B) with intron start sites and strong positional correlation of CAGE clusters with transcription termination sites (panel C). Both observations were relevant only when the CAGE clusters and genes were on the same strand, further supporting a meaningful biological relationship. More detailed analysis showed very precise localization of CAGE clusters at donor sites and at polyadenylation sites (Fig. S4D). To check statistical significance of this observation, we selected equivalent random positions at 500 bp downstream from the donor splice sites or polyadenylation sites, as a control set. The resulting contingency tables presented in the Table S2. The Exact Fisher test for these contingency tables gave p-values less than $2.2 \cdot 10^{-16}$ in both cases.

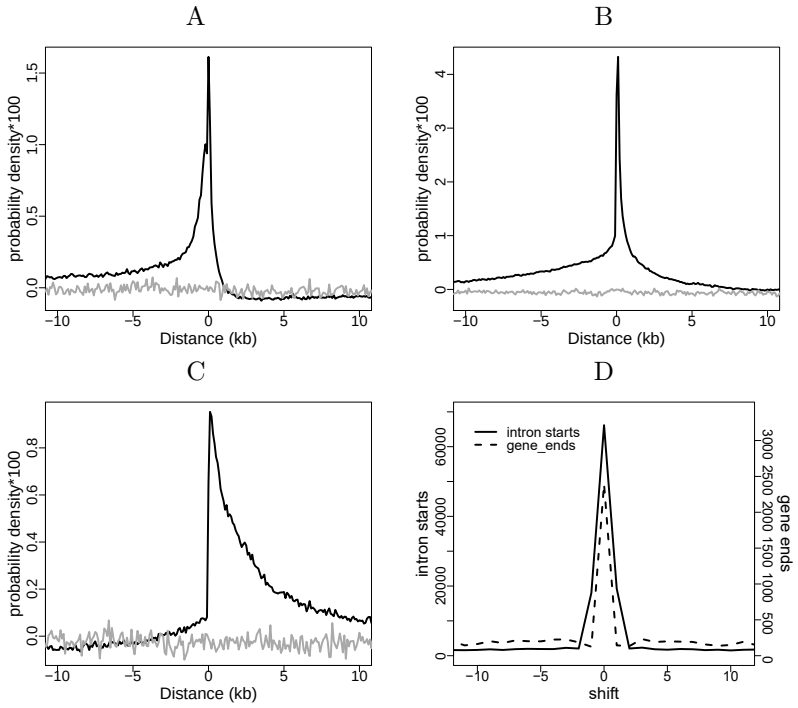

Figure S4: The cross-correlation functions for CAGE vs gene annotation. Grey lines show background (shuffled windows), solid lines show foreground (matched windows). A. CAGE vs gene starts; B. CAGE vs intron starts; C. CAGE vs gene ends; D. CAGE vs intron starts (solid line) and gene ends (dashed line) at single nucleotide resolution.

Table S2: Contingency tables for numbers of CAGE clusters starting at specific positions in comparison with +500bp control position.

Donor splice site

	CAGE	no CAGE
intron start	66181	320252
intron start+500	50	386383
p-value	$< 2.2 \cdot 10^{-16}$	

Poly-A sites

	CAGE	no CAGE
gene end	2393	42003
gene end+500	2	44394
p-value	$< 2.2 \cdot 10^{-16}$	

7 Epigenomic data from modENCODE

As presented in the paper (Zhou and Troyanskaya, 2014) we take the data for the cell line S2-DRSC (http://flybase.org/reports/FBtc0000181.html) from the last version of modENCODE. The modENCODE for this cell line contains only tracks with the chromatin marks and with the chromatin modification complexes. We run the *StereoGene* for all pairs of factors presented in table 2 in the cited paper. The results for these pairs presented in the table S3.

Table S3: Comparison of the Kerneled Correlation (KC) and the Interaction energy score (IES)

Assay Factor1	Assay Factor2	KC	IES
H4K16ac	MSL-1	0.75	5.1
MOF	MSL-1	0.70	4.56
H3K9me2	H3K9me3	0.90	4.53
HP1b	HP1c	0.95	4.21
dSFMBT	Pho	0.80	3.76
H3K27me3	Pc	0.69	3.52
dRING	Pc	0.78	3.5
H3K9me3	HP1a	0.78	3.21
CP190	mod(mdg4)	0.59	3.1
H3K9me3	Su(var)3-9	0.80	3.05
JIL-1	MSL-1	0.60	2.64
CP190	Su(Hw)	0.46	2.64
HP1a	HP4	0.26	2.58
H3K36me3	JIL-1	0.87	2.56
mod(mdg4)	Su(Hw)	0.59	2.49
H2Bubi	H3K79me2	0.88	2.45
Enhancer-of-zeste	Pc	0.77	2.43
HP1a	HP2	0.56	2.42
GAF	MOF	0.61	2.4
H3	H3K23ac	0.30	2.29

To get more detailed picture we present a heat-map for the Kernel Correlation for all possible pairs from the set (Figure S5). On this map one can see several clusters:

- Insulator-related cluster: Su(hw), mod(mod4), CP190;
- Polycomb-related cluster: H3K23ac, H3K27me3, Enhancer.of.zeste, dRING, Pc;
- Large cluster related to active chromatine: H2Bubi, H3K79me2, JIL.1, H3K36me3;
- Histone acetylation: MOF, H4K16ac, MSL.1
- Polycomb response elements: MOF, GAF, dSFMBT, Pho;
- Heterochromatine: HP1b, HP1c;
- Heterochromatine: HP4, HP2,HP1a, Su.var.3.9, H3K9me2, H3K9me3

Seems to be strange existing acetylated histone H3K23ac in the same cluster with repressed polycomb-related features. Nevertheless, in the paper (Fu Huang et. al, Genes & development, 2014) mentioned that this histone modification is related to polycomb system: "The H3K23 residue has been shown to stabilize the interaction between H3K27me3 and the chromodomain of Polycomb (Fischle et al. 2003). Therefore, acetylation of H3K23 may affect the recognition of H3K27me3 by the Polycomb complex".

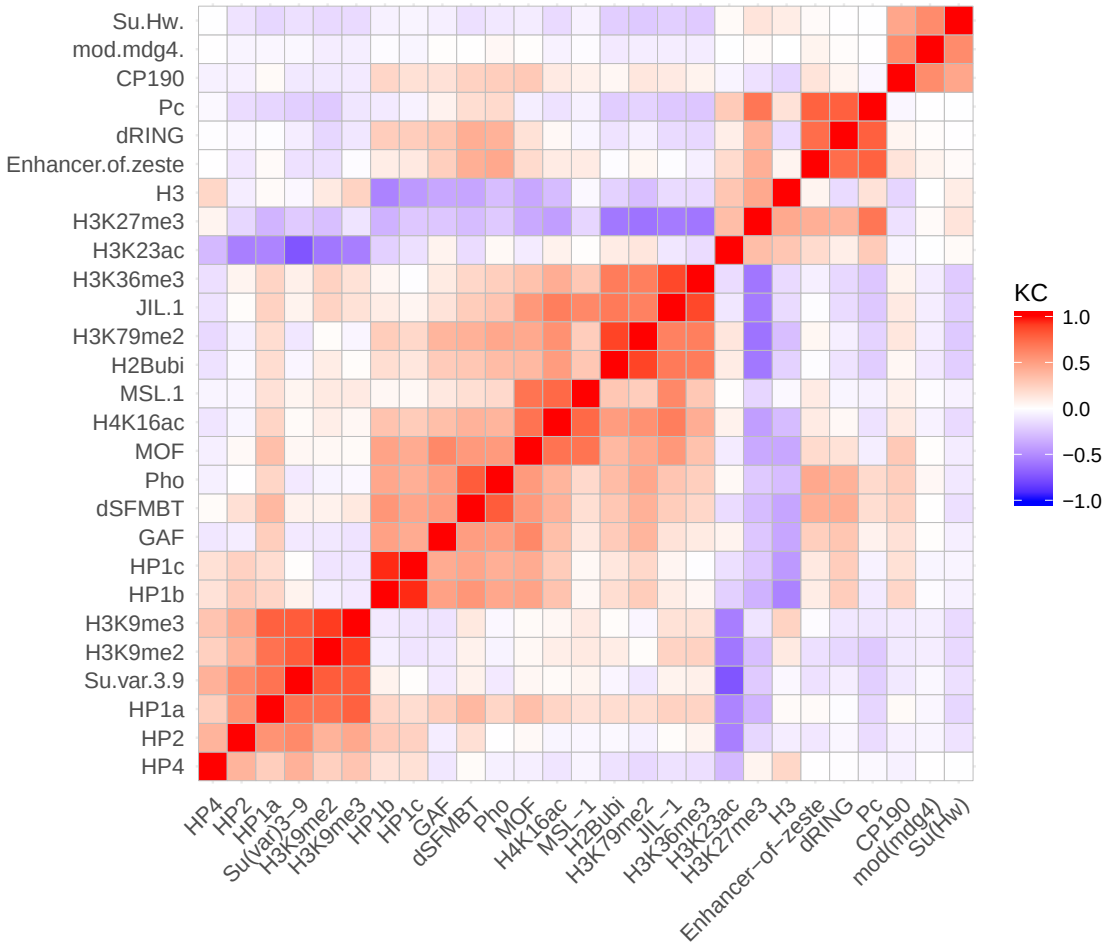

Figure S5: Heatmap for kernel correlations for all pairs of factors from the table S3

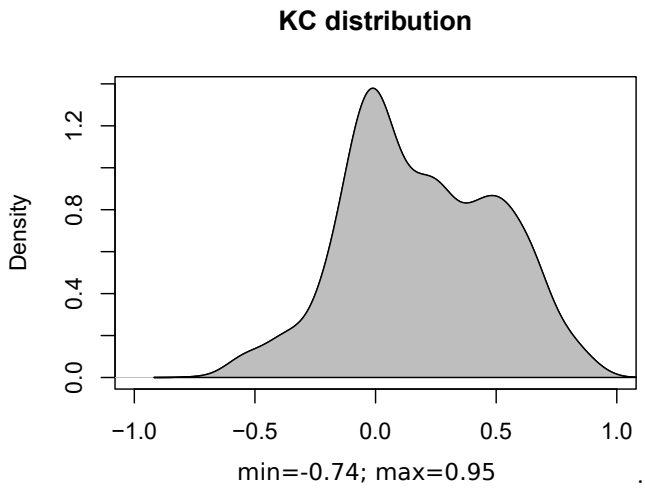

Figure S6: The distribution of the KC density.

The distribution of the KC density over all 2211 comparisons presented on the Fig.S6. The minimal value of the KC (-0.74) reached on comparison H3K23ac vs Su(var)3-9; the maximal value (0.95) was obtained on the comparison HP1b vs HP1c.

8 The Peak at zero position in the cross-correlation function

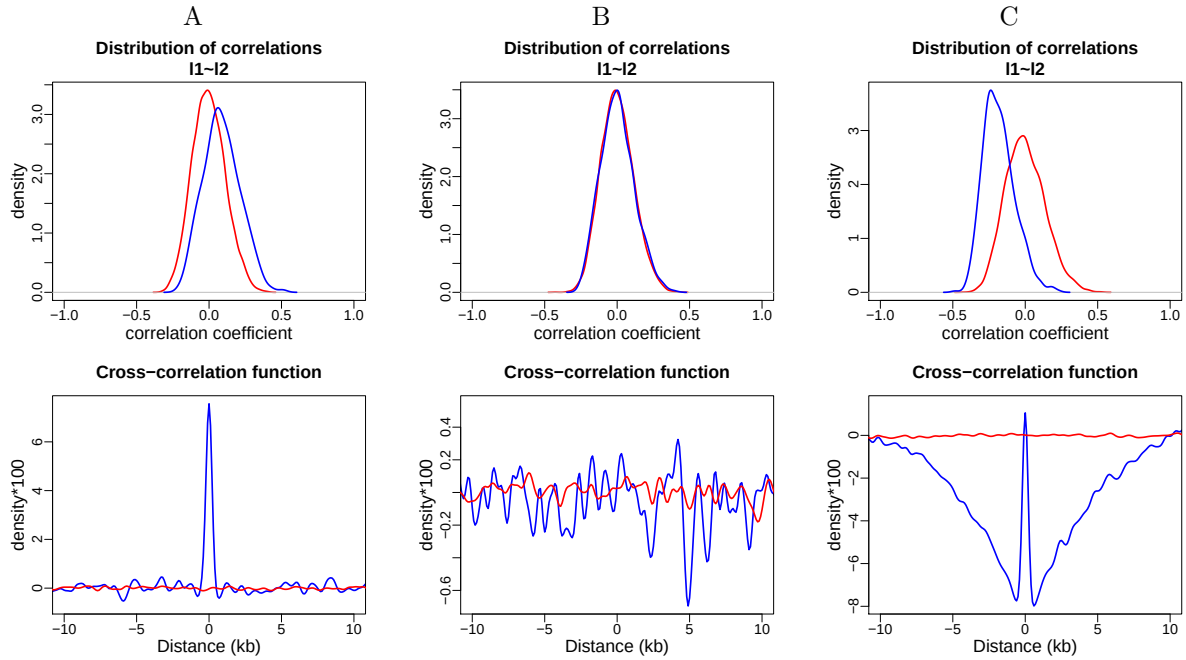

Figure S7: A. Correlation distribution and cross-correlation function for two random marks located on 'nucleosomes'. B. The same for two tracks generated independently. C. The same, but for Markov model of track generation. As usual upper plot shows the correlation distribution, the lower plot – the cross-correlation function; red lines – background distributions; blue lines observed distributions.

In many cases, we observe a high peak at zero position in the cross-correlation function (see for example Fig. S1A) even when the correlation coefficient is about zero or negative. We hypothesize that this peak is related to exact nucleosome positioning. To check these hypotheses we generate an artificial 'genome' of length 60 Mb and place to this genome 10000 'nucleosomes'. Every nucleosome may have no marks (type 0), may have mark1 (type 1), may have mark2 (type2) or may have two marks (type 3). We assign randomly the nucleosomes to one of defined types with probabilities:

type 0	type 1	type 2	type 3
0.15	0.4	0.4	0.05

Then we generated signals for two marks. The signal has a gaussian form with center at the 'nucleosome':

$$value(x) = \sum_{nucleosomes} \xi * exp(-\frac{(x - pos_i)^2}{\sigma^2}$$

where $value$ – signal level; ξ – a random value distributed exponentially with $\lambda = 8$; $\sigma = 100$ – width of the signal on the nucleosome; pos_i – position of i-th nucleosome. We run the *StereoGene* on these tracks and obtain correlation distribution and the cross-correlation (Fig. S7A). As a control we generate two independent set of nucleosomes and create and analyzed two tracks (Fig. S7B). To create a more realistic model we use a Markov model for nucleosome state generation. Using following transition probability matrix

	type 0	type 1	type 2	type 3
type 0	0.30	0.30	0.30	0.10
type 1	0.10	0.80	0.05	0.05
type 2	0.10	0.05	0.80	0.05
type 3	0.15	0.35	0.35	0.15

we create two tracks. The probability distribution of the states remain the same as for previous cases. Nevertheless, the cross-correlation function became more realistic (Fig. S7C).

9 The correlation analysis for the binarized data

To analyze the influence of the data binarization on the correlation values we produce binarized tracks using the following procedure. We define the maximal observed value of a track. We write a maximal value to the output track if the input value is greater than the selected threshold; we write zero otherwise. Then, we run our program on the binarized tracks. We used the H3K27me3 and H3K36me3 tracks for the Fetal brain cells. The results are presented in the Fig. S8. We see that binarization dramatically changes the results – the correlation coefficients vary from very high positive value to negative value (Fig. S8A). The correlation distributions and cross-correlation function Fig. S8B) that are obtained with the reasonable 50% threshold are dramatically different from the distributions obtained on continues data (see Fig. S1). Moreover, the binarization forced the correlation distribution to be strongly multimodal, that actually means that the data structure is broken.

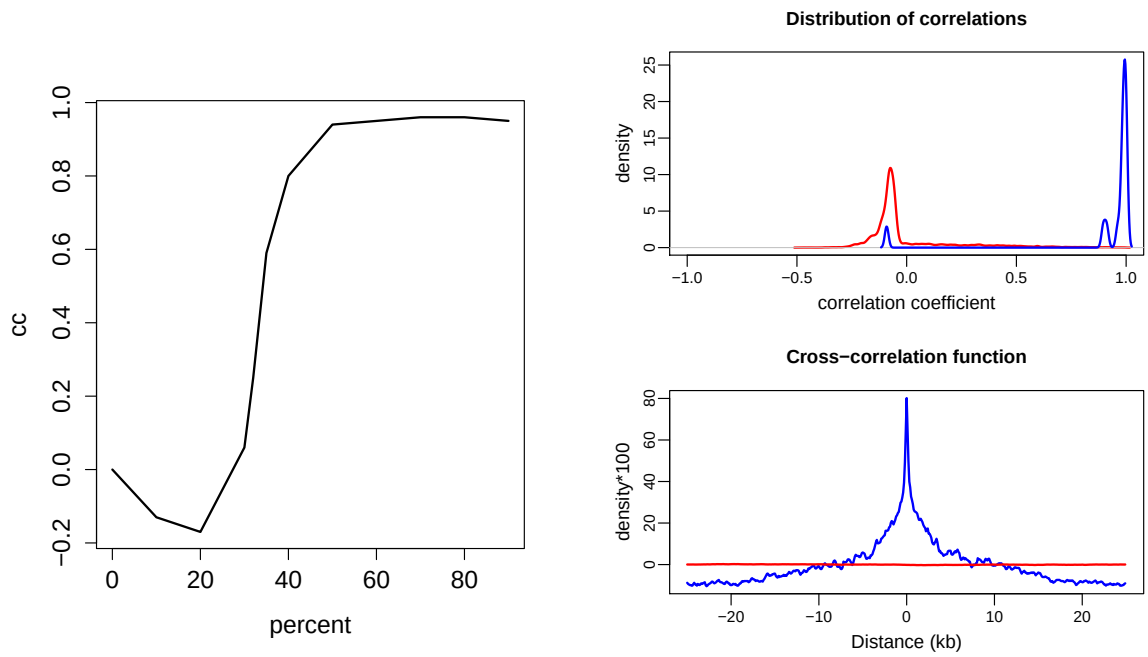

Figure S8: Left – dependence of the KC on binarization threshold. X-axis – threshold in percent of the maximum observed value in the profile; Y-axis – the KC value. Right – distribution of the KC over the windows (upper plot) and cross-correlation (lower plot) for binarized profiles for the threshold value = 50% of max value. The data is the same as on Fig. S1

10 Data used

Table S4: List of used fetal and adult tissues used in the Fig.1 in the main text

Fetal tissues	Adult tissues
	Adipose Nuclei
	Adipose Tissue
	Adrenal Gland
Fetal Adrenal Gland	Adult Kidney
Fetal Brain	Adult Liver
Fetal Heart	Aorta
Fetal Intestine Large	Bladder
Fetal Intestine Small	Brain Angular Gyrus
Fetal Kidney	Brain Anterior Caudate
Fetal Kidney Left	Brain Cingulate Gyrus
Fetal Kidney Right	Brain Germinal Matrix
Fetal Lung	Brain Hippocampus Middle
Fetal Lung Left	Brain Inferior Temporal Lobe
Fetal Lung Right	Brain Mid Frontal Lobe
Fetal Muscle Arm	Brain Substantia Nigra
Fetal Muscle Back	Colonic Mucosa
Fetal Muscle Leg	Colon Smooth Muscle
Fetal Muscle Lower Limb	Duodenum Mucosa
Fetal Muscle Trunk	Duodenum Smooth Muscle
Fetal Muscle Upper Limb	Esophagus
Fetal Ovary	Gastric
Fetal Placenta	Left Ventricle
Fetal Renal Cortex	Lung
Fetal Renal Cortex Left	Ovary
Fetal Renal Cortex Right	Pancreas
Fetal Renal Pelvis	Pancreatic Islets
Fetal Renal Pelvis Left	Placenta Amnion
Fetal Renal Pelvis Right	Placenta Basal Plate
Fetal Spinal Cord	Placenta Chorion Smooth
Fetal Stomach	Placenta Villi
Fetal Testes	Primary Fibroblast
Fetal Thymus	Psoas Muscle
Fibroblasts Fetal Skin Abdomen	Rectal Mucosa
Fibroblasts Fetal Skin Back	Rectal Smooth Muscle
Fibroblasts Fetal Skin Biceps Left	Right Atrium
Fibroblasts Fetal Skin Biceps Right	Right Ventricle
Fibroblasts Fetal Skin Quadriceps Left	Sigmoid Colon
Fibroblasts Fetal Skin Quadriceps Right	Skeletal Muscle
Fibroblasts Fetal Skin Scalp	Small Intestine
Fibroblasts Fetal Skin Upper Back	Spleen
	Stomach Mucosa
	Stomach Smooth Muscle
	Thymus

Table S5: Data sources for the main text

GSM849326 CAGE nucleous plus strand (https://www.ncbi.nlm.nih.gov/geo/download/?acc=GSM849326&format=file&file=GSM849326%5Fhg19%5FwgEncodeRikenCageH1hescNucleusPapPlusSignalRep2%2EbigWig)
GSM849356 CAGE cytosol plus strand (https://www.ncbi.nlm.nih.gov/geo/download/?acc=GSM849356&format=file&file=GSM849356%5Fhg19%5FwgEncodeRikenCageH1hescCytosolPapPlusSignalRep2%2EbigWig)
GSM849326 CAGE nucleous minus strand (https://www.ncbi.nlm.nih.gov/geo/download/?acc=GSM849326&format=file&file=GSM849326%5Fhg19%5FwgEncodeRikenCageH1hescNucleusPapMinusSignalRep2%2EbigWig)
GSM849356 CAGE cytosol minus strand (https://www.ncbi.nlm.nih.gov/geo/download/?acc=GSM849356&format=file&file=GSM849356%5Fhg19%5FwgEncodeRikenCageH1hescCytosolPapMinusSignalRep2%2EbigWig)
GSM751275 Brain Hippocampus Middle, mRNA-Seq for cage test (only active genes were selected) (https://www.genboree.org/EdaccData/Current-Release/experiment-sample/mRNA-Seq/Brain_Germinal_Matrix/UCSF-UBC.Brain_Germinal_Matrix.mRNA-Seq.HuFGM02.wig.gz)
GSM621405 Fetal Lung from Human Epigenome Atlas, H3K4me3 (https://www.genboree.org/EdaccData/Current-Release/experiment-sample/Histone_H3K4me3/Fetal_Lung/BI.Fetal_Lung.H3K4me3.UW_H-22676.wig.gz)
GSM621405 Fetal Lung from Human Epigenome Atlas, H3K27me3 (https://www.genboree.org/EdaccData/Current-Release/experiment-sample/Histone_H3K27me3/Fetal_Lung/BI.Fetal_Lung.H3K27me3.UW_H-22727.wig.gz)
GSM915336 Lung from Human Epigenome Atlas, H3K4me3 (https://www.genboree.org/EdaccData/Current-Release/experiment-sample/Histone_H3K4me3/Lung/UCSD.Lung.H3K4me3.STL002.wig.gz)
GSM1220283 Lung from Human Epigenome Atlas, H3K27me3 (https://www.genboree.org/EdaccData/Current-Release/experiment-sample/Histone_H3K27me3/Lung/UCSD.Lung.H3K27me3.STL002.wig.gz)
GSM438363 Strand-specific, shotgun sequencing of mRNA from the IMR90 cell line; mRNA-seq_imr90_r1 (https://www.ncbi.nlm.nih.gov/geo/download/?acc=GSM438363&format=file&file=GSM438363%5FUCSD%2EIMR90%2EmRNA%2DSeq%2EmRNA%2Dseq%5Fimr90%5Fr1%2Ewig%2Egz)
GSM935513 Stanford_ChipSeq_IMR90_Pol2_IgG-rab (https://www.ncbi.nlm.nih.gov/geo/download/?acc=GSM935513&format=file&file=GSM935513%5Fhg19%5FwgEncodeSydhTfbsImr90Pol2IggrabSig%2EbigWig)

Table S6: Data for Fig.3 in the main text

GSM916038 Brain Hippocampus Middle, H3K27me3 (https://www.genboree.org/EdaccData/Current-Release/experiment-sample/Histone_H3K27me3/Brain_Hippocampus_Middle/BI.Brain_Hippocampus_Middle.H3K27me3.150.wig.gz)
GSM916040 Brain Hippocampus Middle, H3K4me3 (https://www.genboree.org/EdaccData/Current-Release/experiment-sample/Histone_H3K4me3/Brain_Hippocampus_Middle/BI.Brain_Hippocampus_Middle.H3K4me3.150.wig.gz)
GSM751275 Brain Hippocampus Middle, mRNA-Seq (https://www.genboree.org/EdaccData/Current-Release/experiment-sample/mRNA-Seq/Brain_Germinal_Matrix/UCSF-UBC.Brain_Germinal_Matrix.mRNA-Seq.HuFGM02.wig.gz)

Table S7: Data used in the supplementary Fig S2

GSM773007 Brain Cingulate Gyrus, H3K4me1 (https://www.genboree.org/EdaccData/Current-Release/sample-experiment/Brain_Cingulate_Gyrus/Histone_H3K4me1/BI.Brain_Cingulate_Gyrus.H3K4me1.149.wig.gz)
GSM773008 Brain Cingulate Gyrus, H3K4me3 (https://www.genboree.org/EdaccData/Current-Release/sample-experiment/Brain_Cingulate_Gyrus/Histone_H3K4me3/BI.Brain_Cingulate_Gyrus.H3K4me3.149.wig.gz)
GSM670032 Brain Cingulate Gyrus, H3K9ac (https://www.genboree.org/EdaccData/Current-Release/sample-experiment/Brain_Cingulate_Gyrus/Histone_H3K9ac/BI.Brain_Cingulate_Gyrus.H3K9ac.112.wig.gz)
GSM772989 Brain Cingulate Gyrus, H3K27me3 (https://www.genboree.org/EdaccData/Current-Release/sample-experiment/Brain_Cingulate_Gyrus/Histone_H3K27me3/BI.Brain_Cingulate_Gyrus.H3K27me3.149.wig.gz)
GSM773009 Brain Cingulate Gyrus, H3K36me3 (https://www.genboree.org/EdaccData/Current-Release/sample-experiment/Brain_Cingulate_Gyrus/Histone_H3K36me3/BI.Brain_Cingulate_Gyrus.H3K36me3.149.wig.gz)

Table S8: Data used in the supplementary table S1

GSM1003585	H1-hesc,	H3K9me3	(http://hgdownload.cse.ucsc.edu/goldenPath/hg19/encodeDCC/wgEncodeBroadHistone/wgEncodeBroadHistoneH1hescH3k09me3StdSig.bigWig)
GSM733725	H1-hesc,	H3k36me3	(http://hgdownload.cse.ucsc.edu/goldenPath/hg19/encodeDCC/wgEncodeBroadHistone/wgEncodeBroadHistoneH1hescH3k36me3StdSig.bigWig)
GSM1003547	H1-hesc,	H3k79me2	(http://hgdownload.cse.ucsc.edu/goldenPath/hg19/encodeDCC/wgEncodeBroadHistone/wgEncodeBroadHistoneH1hescH3k79me2StdSig.bigWig)
GSM733748	H1-hesc,	H3K27me3	(http://hgdownload.cse.ucsc.edu/goldenPath/hg19/encodeDCC/wgEncodeBroadHistone/wgEncodeBroadHistoneH1hescH3k27me3StdSig.bigWig)
GSM733687	H1-hesc,	H4k20me1	(http://hgdownload.cse.ucsc.edu/goldenPath/hg19/encodeDCC/wgEncodeBroadHistone/wgEncodeBroadHistoneH1hescH4k20me1StdSig.bigWig)
GSM733718	H1-hesc,	H3k27ac	(http://hgdownload.cse.ucsc.edu/goldenPath/hg19/encodeDCC/wgEncodeBroadHistone/wgEncodeBroadHistoneH1hescH3k27acStdSig.bigWig)
GSM733657	H1-hesc,	H3k4me3	(http://hgdownload.cse.ucsc.edu/goldenPath/hg19/encodeDCC/wgEncodeBroadHistone/wgEncodeBroadHistoneH1hescH3k4me3StdSig.bigWig)
GSM733773	H1-hesc,	H3k9ac	(http://hgdownload.cse.ucsc.edu/goldenPath/hg19/encodeDCC/wgEncodeBroadHistone/wgEncodeBroadHistoneH1hescH3k9acStdSig.bigWig)
GSM733670	H1-hesc,	H3k4me2	(http://hgdownload.cse.ucsc.edu/goldenPath/hg19/encodeDCC/wgEncodeBroadHistone/wgEncodeBroadHistoneH1hescH3k4me2StdSig.bigWig)
GSM733782	H1-hesc,	H3k4me1	(http://hgdownload.cse.ucsc.edu/goldenPath/hg19/encodeDCC/wgEncodeBroadHistone/wgEncodeBroadHistoneH1hescH3k4me1StdSig.bigWig)
GSM1003579	H1-hesc,	H2AZ	(http://hgdownload.cse.ucsc.edu/goldenPath/hg19/encodeDCC/wgEncodeBroadHistone/wgEncodeBroadHistoneH1hescH2azStdSig.bigWig)
GSM803466	H1-hesc,	Rad21	(http://hgdownload.cse.ucsc.edu/goldenPath/hg19/encodeDCC/wgEncodeHaibTfbs/wgEncodeHaibTfbsH1hescRad21V0416102RawRep1.bigWig)
GSM803419	H1-hesc,	CTCF	(http://hgdownload.cse.ucsc.edu/goldenPath/hg19/encodeDCC/wgEncodeHaibTfbs/wgEncodeHaibTfbsH1hescCtcfsc5916V0416102RawRep1.bigWig)
GSM945302	K562,	H3k36me3	(http://hgdownload.cse.ucsc.edu/goldenPath/hg19/encodeDCC/wgEncodeUwHistone/wgEncodeUwHistoneK562H3k36me3StdRawRep1.bigWig)
GSM945228	K562,	H3K27me3	(http://hgdownload.cse.ucsc.edu/goldenPath/hg19/encodeDCC/wgEncodeUwHistone/wgEncodeUwHistoneK562H3k27me3StdPkRep1.narrowPeak.gz)
GSM733776	K562,	H3K9me3	(http://hgdownload.cse.ucsc.edu/goldenPath/hg19/encodeDCC/wgEncodeBroadHistone/wgEncodeBroadHistoneK562H3k9me3StdSig.bigWig)
GSM733653	K562,	H3k79me2	(http://hgdownload.cse.ucsc.edu/goldenPath/hg19/encodeDCC/wgEncodeBroadHistone/wgEncodeBroadHistoneK562H3k79me2StdSig.bigWig)
GSM733656	K562,	H3k27ac	(http://hgdownload.cse.ucsc.edu/goldenPath/hg19/encodeDCC/wgEncodeBroadHistone/wgEncodeBroadHistoneK562H3k27acStdSig.bigWig)
GSM733778	K562,	H3k9ac	(http://hgdownload.cse.ucsc.edu/goldenPath/hg19/encodeDCC/wgEncodeBroadHistone/wgEncodeBroadHistoneK562H3k9acStdSig.bigWig)
GSM733777	K562,	H3K9me1	(http://hgdownload.cse.ucsc.edu/goldenPath/hg19/encodeDCC/wgEncodeBroadHistone/wgEncodeBroadHistoneK562H3k9me1StdSig.bigWig)
GSM733680	K562,	H3k4me3	(http://hgdownload.cse.ucsc.edu/goldenPath/hg19/encodeDCC/wgEncodeBroadHistone/wgEncodeBroadHistoneK562H3k4me3StdSig.bigWig)
GSM733675	K562,	H4k20me1	(http://hgdownload.cse.ucsc.edu/goldenPath/hg19/encodeDCC/wgEncodeBroadHistone/wgEncodeBroadHistoneK562H4k20me1StdSig.bigWig)
GSM733651	K562,	H3k4me2	(http://hgdownload.cse.ucsc.edu/goldenPath/hg19/encodeDCC/wgEncodeBroadHistone/wgEncodeBroadHistoneK562H3k4me2StdSig.bigWig)
GSM733692	K562,	H3k4me1	(http://hgdownload.cse.ucsc.edu/goldenPath/hg19/encodeDCC/wgEncodeBroadHistone/wgEncodeBroadHistoneK562H3k4me1StdSig.bigWig)
GSM733786	K562,	H2AZ	(http://hgdownload.cse.ucsc.edu/goldenPath/hg19/encodeDCC/wgEncodeBroadHistone/wgEncodeBroadHistoneK562H2azStdSig.bigWig)
GSM803447	K562,	Rad21	(http://hgdownload.cse.ucsc.edu/goldenPath/hg19/encodeDCC/wgEncodeHaibTfbs/wgEncodeHaibTfbsK562Rad21V0416102RawRep1.bigWig)
GSM1010820	K562,	CTCF	(http://hgdownload.cse.ucsc.edu/goldenPath/hg19/encodeDCC/wgEncodeHaibTfbs/wgEncodeHaibTfbsK562CtcfcPcr1xRawRep1V2.bigWig)